Influence of $K_3Fe(CN)_6$ on the electrochemical performance of carbon derived from waste tyres by K_2CO_3 activation

A. Bello[1, 2], D. Y. Momodu[2], M. J. Madito[2], K Makgopa[3], Khavharendwe M. Rambau[4], Julien Dangbegno[2] Nicholas M. Musyoka[4] and N. Manyala[2*]

[1]Department of Materials Science and Engineering, African University of Science and Technology (AUST), Abuja, Nigeria

[2]Department of Physics, Institute of Applied Materials, SARCHI Chair in Carbon Technology and Materials, University of Pretoria, Pretoria 0028, South Africa.

[3]Department of Chemistry, Tshwane University of Technology, Pretoria 0001, South Africa.

[4]HySA Infrastructure Center of Competence, Materials Science and Manufacturing Council for Scientific and Industrial Research (CSIR), Meiring Naude Road, Brummeria, 395 Pretoria, 0001, South Africa

[*]Email address: ncholu.manyala@up.ac.za (N. Manyala)

Corresponding author Tel: +27 (0)12 420 3549, Fax: +27 (0)12 420 2516

Highlights

- ✓ Revalorisation of waste tyres as a means to sustainable value added porous carbon.
- ✓ K_2CO_3 activation and carbonization of the hydrochar to produce porous carbons.
- ✓ Electrodes based on the porous carbon exhibit good electrochemical performance.
- ✓ Investigate the influence of redox-mediated electrolytes on the porous carbon.

Abstract

Revalorisation of waste tyres to sustainable value added carbons was studied as a possible means of addressing the challenges with rising demand for energy across the globe. Crumble tyres were used for the production of activated carbon (AC) in the presence of potassium carbonate (K_2CO_3) salt as the activating agent. The activated carbon (AC) materials exhibited predominantly mesoporous framework with specific surface area between 147 and 385 $m^2\ g^{-1}$. Fabricated electrodes from these AC materials displayed a discharge capacity of 50 mAh g^{-1} at 0.25 A g^{-1} in a redox-mediated electrolyte of 1 M $K_3Fe(CN)_6$-1 M HNO_3 corresponding to a specific capacitance of 140 F g^{-1} at the same specific

current, with an energy efficiency of 70% after 1000 cycles. The enhanced electrochemical performance of the electrode is due to a coupling electrolyte additive, which offers an alternative approach for the design of an efficient electrochemical energy storage device.

KEY WORDS: Waste tyres, Porous carbon, Redox-mediated electrolyte, Supercapacitors, Electrochemical Properties

Graphical Abstract

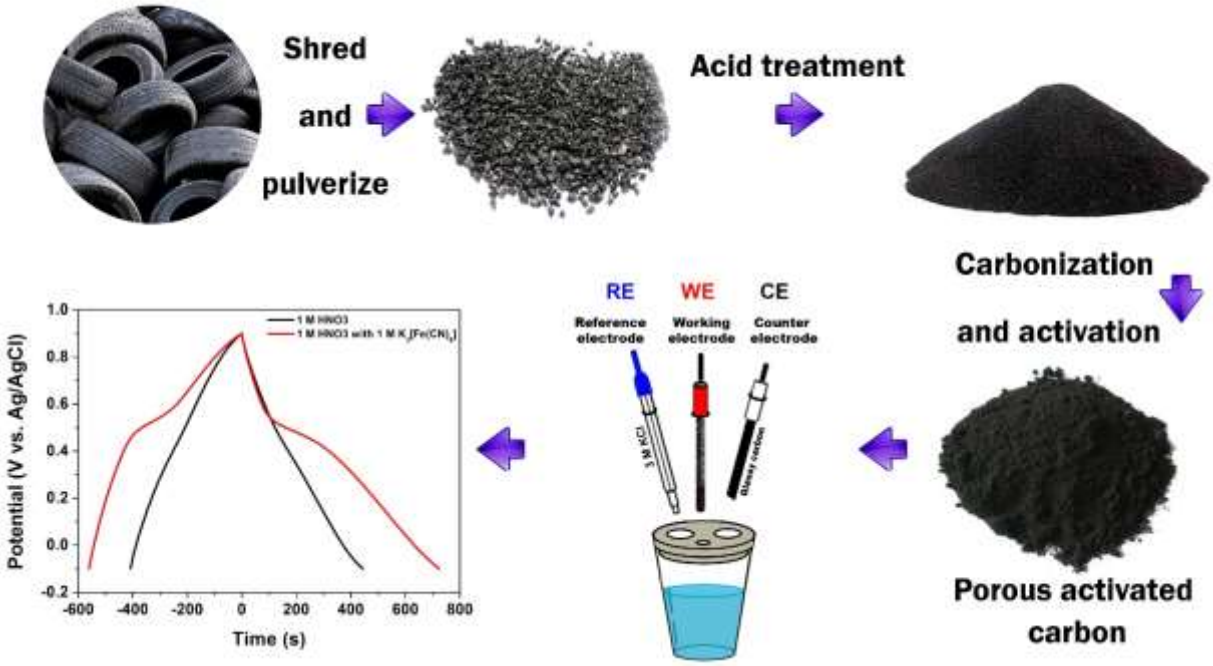

1. Introduction

Tyres are made from petroleum products and usually designed to withstand extreme conditions (very resistant and non-biodegradable), hence making recycling very challenging. The non-biodegradable natures of tyres make their disposal very difficult, always floating on landfill locations and constitute waste materials that pose risk to the environment. Every year millions of tyres are produced globally due to massive growth in the use and manufacture of vehicles, which will eventually lead to a global solid waste problem,

resulting in unprecedented energy wastage. Thus, many research efforts have been focused on the revalorization and recovery of energy from waste tyres, from both environmental and economic perspective. Generally, waste tyres can be classified as a biomass renewable energy resource which are low cost, sustainable and environmentally friendly sources of materials for the development of efficient electrodes for energy storage technology such as supercapacitor [1–4]. Carbon is the major constituent of tyres with a substantial amount of organic materials such as natural rubber, polybutadiene, styrene butadiene rubber and butyl rubber [2]. Therefore, reclamation of the carbon content for value-added use such as electrodes in supercapacitors and batteries would be beneficial, taking advantage of the unusable and wasted energy locked in waste tyres. Retrieval of the carbon content is usually done through a pyrolysis process which produces a carbon material (char), in addition to the oil and gas that provide the energy that drives the pyrolysis process [5]. However, the carbon material produced by this technique is often limited in surface area which might not be suitable for practical applications as electrodes in electrochemical energy storage devices. Hence, they are often activated physically via carbon dioxide (CO_2) to develop porosity in the carbon material [5]. For example, activated carbon (AC) with a specific surface area (SSA) of 414 $m^2 g^{-1}$ at 900 ^oC with a flow rate 150 mL/min of CO_2 and reaction time of 180 min was reported by Betancur et al. [5]. Similarly, a maximum SSA of 432 $m^2 g^{-1}$ was reported for a water steam (H_2O/CO_2) oxidizing atmosphere with varying time between 120–150 min at 970 °C and at a burn-off level of 60–65 wt.% [6]. The N_2 atmosphere recuperated carbon as anode material demonstrated a reversible capacity of 390 mA h g^{-1} with ~100% coulombic efficiency [7]. Recently, chemical activation has been shown to be an effective method to obtain AC with high SSA and slit micropore distribution and hence very attractive. Different activating agents including KOH [8], $ZnCl_2$ [9], H_3PO_4 [10,11], NaOH [12],

have been explored. It has been shown recently that KOH-activated carbon from waste tyres and polymer composite (i.e., PANI) demonstrated a high SSA of 1625 m^2 g^{-1} with a specific capacitance (C_{SP}) of 480 F g^{-1} at 1 mV s^{-1} [2]. The effect of H_3PO_4 activation process on porosity and structure of AC supercapacitor electrode materials from scrap waste tyres was also reported [11]. The obtained AC materials demonstrated SSA ranging from 208.5 m^2 g^{-1} - 563.2 m^2 g^{-1} with different activation ratio and temperatures, the electrodes fabricated displaying C_{SP} between 42 F g^{-1} - 106.4 F g^{-1}, rate capability ranging between 0.784-0.723. The authors concluded that ion diffusion is the rate-limiting factor for the rate capability of AC electrodes [11]. In this work, we interrogate and explore the feasibility and production of activated carbon from waste tyres using a benign alkaline salt; K_2CO_3 which is relatively not a hazardous chemical and not deleterious as it is frequently used for food additives compared to H_3PO_4 and KOH which are both corrosive. Taking into account that there are few reports on this, the main objective of this work is to elucidate the ratio of AC from scrap tyre and K_2CO_3 as an activating agent. Taking into account the integration of various voltage windows concerning the redox additives and we study the influences of the activation ratio on the electrochemical performance of the fabricated electrodes for supercapacitors in redox-mediated electrolytes. We assembled them into a novel redox system; namely, the $K_3Fe(CN)_6$-1 M HNO_3 aqueous electrolyte, primarily owing to the solubility between them. Furthermore, the effect of molar ratio of $K_3Fe(CN)_6$ on the capacitive behaviour was emphatically by a series of electrochemical analysis.

2. Methods

2.1 Experiment

Waste tyres were used as the starting material for the production of activated carbon (AC) presented in this work. The crumbled tyre was acid treated and pyrolysed to carbon by following the procedure reported by Boota et al. [2]. The obtained carbon material was divided into five samples which were then activated using a mild alkaline carbonate salt (K_2CO_3) with varying weight ratio of the carbon/K_2CO_3 = 2, 4, 6, 8 and 10. Each of the samples was physically mixed in an agate mortar to impregnate the carbon materials with K_2CO_3 powder. The samples were then transferred into a horizontal tube furnace and activated at 800 °C under N_2 flow for 1 h, followed by washing until a neutral pH was attained. The materials were labelled according to the ratio of the carbon and activating agent (e.g. sample 1 corresponds to a 1:2 ratio of the carbon and K_2CO_3 respectively).

2.2. Materials characterization

A Zeiss Ultra Plus 55 field emission scanning electron microscope (FE-SEM) was used to study the morphology of the produced AC. The crystallographic analysis was carried on an XPERT-PRO diffractometer and Raman spectroscopy on T64000 spectrometer from HORIBA, (532 nm). All the samples were excited with a 514 nm argon laser line with a laser power of 1.5 mW to avoid possible thermal effects. Fourier transform infrared spectroscopy (FTIR) spectra data are recorded on a Vertex 70v (Bruker) spectrometer. Nitrogen adsorption/desorption measurements were conducted at −196 °C on a Micromeritics ASAP 2020 (version 2.00) analyser. All the samples were initially degassed at 180 °C for more than 12 h under high vacuum conditions.

2.3. Electrochemical measurements

The preparation of electrodes was done by mixing the AC, with acetylene black and Polyvinylidene fluoride (PVdF) in the ratio of 80:10:10 respectively, using pestle and mortar and N-methyl pyrrolidone (NMP) solution to form a slurry. From the slurry a uniform coating with a thickness of 0.2 mm was coated on a carbon paper (which was used as a current collector) and dried at 60 °C. The electrochemical measurements were carried out in a three-electrode configuration with a glassy carbon counter electrode and Ag/AgCl as reference electrode in various aqueous electrolytes (i.e., 1 M KNO_3, 1 M HNO_3 and 1 M HNO_3 -1 M $K_3[Fe(CN)]_6$). The electrochemical experiments were carried out using a 40-mL cylindrical cell. During the process of optimization, various concentrations of the $K_3[Fe(CN)]_6$ were prepared and 1 mL of each prepared solution was added to a 1 M concentration of HNO_3, that was used for the analysis of the electrodes. A typical preparation of 1 M $K_3[Fe(CN)]_6$ was carried out by dissolving 6.5848 g of the salt in 20 ml of deionized water. Then 1 mL of the prepared solution was added to 40 mL of 1 M HNO_3 in the cylindrical cell of a fixed volume for all our experiment for better comparison. The electrochemical test was carried out on a Bio-logic VMP-300 potentiostat with techniques such as cyclic voltammetry (CV), galvanostatic cycling with potential limitation (GCPL) and the electrochemical impedance spectroscopy (EIS). The specific capacitance (C_{SP}) and discharge capacities are evaluated from the CV curves using the equations below [13,14]:

$$C_{\mathrm{SP}} = \frac{\int I \, \mathrm{d}U}{\nu m \Delta U} \qquad 1$$

Or can be calculated from GCD using equation 2

$$C_{\mathrm{SP}} = \frac{I \, \Delta t}{m \, \Delta U} \qquad 2$$

While the discharge capacity Q_D was evaluated using equation 3 from the GCD curves,

$$Q_D = \frac{I\,\Delta t}{m \times 3.6} \qquad 3$$

where I is the current (mA), ΔU is the potential vs. reference electrode, ν is the potential sweep rate (mV s^{-1}), m is the total mass of electrode active material (mg) and the mass of the electrodes ranges between 2- 5 mg, Δt is the discharge time (s), and Q_D is the specific discharge capacity (mA h g^{-1}).

3. Results and Discussion

3.1 Structural and morphological analysis

All the structural and morphological characterizations are presented in the supplementary information (SI). The entire activated carbon (AC) samples of produced showed similar XRD pattern with an amorphous signature (i.e. broad diffraction peaks) at a 2-theta angle of 24° and 42° corresponding to the (002) and (100) crystallographic planes of a carbon material. A representative XRD for the 1:8 sample is shown in Figure S1 (a). Raman data for all the produced samples are shown in Figure S1 (b) with the five samples depicting the well-known D and G peaks which is unique to carbonaceous material [15,16]. The D peak is more pronounced in most of the carbon samples confirming the poor crystallinity and amorphous nature of the produced carbon. The ratio of the (I_D/I_G) is used to determine the degree of defects density of carbon materials and these values are 0.80, 0.81, 0.85, 0.85 and 0.84, respectively for the produced carbon materials. These values confirm that the produced carbons are amorphous in nature with low degree of the graphitization. Figure S1 (c) shows the FTIR spectra of the five samples clearly showing the presence of oxygen functionalities in the carbon material. It can be observed that similar peaks were observed in all five

samples. The peak at ~1658 cm^{-1} is attributed to carbonyl (C=O) groups. The peak at ~1590 cm^{-1} and 1500 cm^{-1} are attributed to C=C vibration mode. Vibration at 1460 cm^{-1} corresponds to $–CH_2$ (alkyl) groups, while peaks at ~1332 cm^{-1} was assigned to the C–O stretching vibrations. An absorption band at ca. 1050 cm^{-1} is attributed to the presence of the R–OH functional groups in the material [17].

A type IV N_2 isotherms was recorded from the BET analysis with a H3 hysteresis loop (see Figure S2 (a)) for all samples according to the IUPAC classification. This corresponds to carbon materials with a porous network consisting of micropores and mesopores which serves as channels and sites for efficient ion-transport and storage respectively [18]. The pore-size distribution (PSD) analysis using the non-local density functional theory (NLDFT) method was performed to study the finite pore geometries from the adsorption isotherms.

Figure S2 (b) shows the PSD plot of all the AC samples with varying activating-agent content. It is observed that the pore size range (0.8 – 2.5 nm) which has the highest pore volume response corresponds to micropores and mesopores. For example, a PSD peak centered at ~1.2 nm with a sharp increase in the pore volume confirms the presence of micropores. Figure S2 (c) shows the BET SSA of the AC at different ratios of the activating agent (K_2CO_3). From the figure, it was observed that the AC SSA increases with increasing impregnation amount of the K_2CO_3. The SSA properties such as BET SSA, and total pore volume are summarized in table S1. This is in total agreement with the observation obtained from the BET plots with the highest pore volume corresponding to the AC-5 sample with a 1:10 ratio. Although, this observed increase in SSA did not correlate with a similar enhancement of the electrochemical performance of the as-fabricated electrode as will be illustrated shortly.

The SEM micrographs of all the produced samples are presented in Figure S3 at high and low magnifications. The figures show that the K_2CO_3 activation of waste tyres leads to the

creation of porous sites within the carbon materials (clearly visible from the high magnification micrographs) with interconnected carbon sheets linked to form a three-dimension structure in the order of several microns. The mechanism of porosity formation with K_2CO_3 involves gasification followed by the removal of CO_2 according to the following set of equations [19];

$$K_2CO_3 + 2C \rightarrow 2K + 3CO \quad (4)$$

$$K_2CO_3 \rightarrow K_2O + CO_2 \quad (5)$$

$$K_2O + 2C \rightarrow 2K + CO \quad (6)$$

Briefly, the activation process leads to the reduction of K_2CO_3 to CO_2, K, K_2O, and CO. The potassium-containing compounds, such as K_2O can be reduced by carbon to form K-metal, which can diffuse into the matrix of the carbon materials, thus enlarging existing pores and forming new pore structures [19,20].

3.2 Electrochemical analysis

Cyclic voltammetry (CV) measurements were carried out on the five electrodes with different ratios of the activating agent to evaluate the charge storage mechanism and capability, in a 1 M HNO_3 electrolyte at 10 and 50 mV s^{-1} within the potential range of -0.1 to +0.9 V vs. Ag/AgCl. Effectively, all the five samples show nearly rectangular CV shapes at both scan rates which is indicative of a double-layer mechanism (Figure 1 (a) and 1 (b)). However, reversible humps located at ~0.3 V vs. Ag/AgCl are observed indicating partial Faradic behavior in both the cathodic and anodic region, which accounts for the Faradic reaction between the protic ion (H^+) and the electrochemical reactions of oxygen surface functionalities as indicated by FTIR. Considering the fact that the oxygen related functionalities are inevitable in carbon-based materials, it is reasonable to conclude that

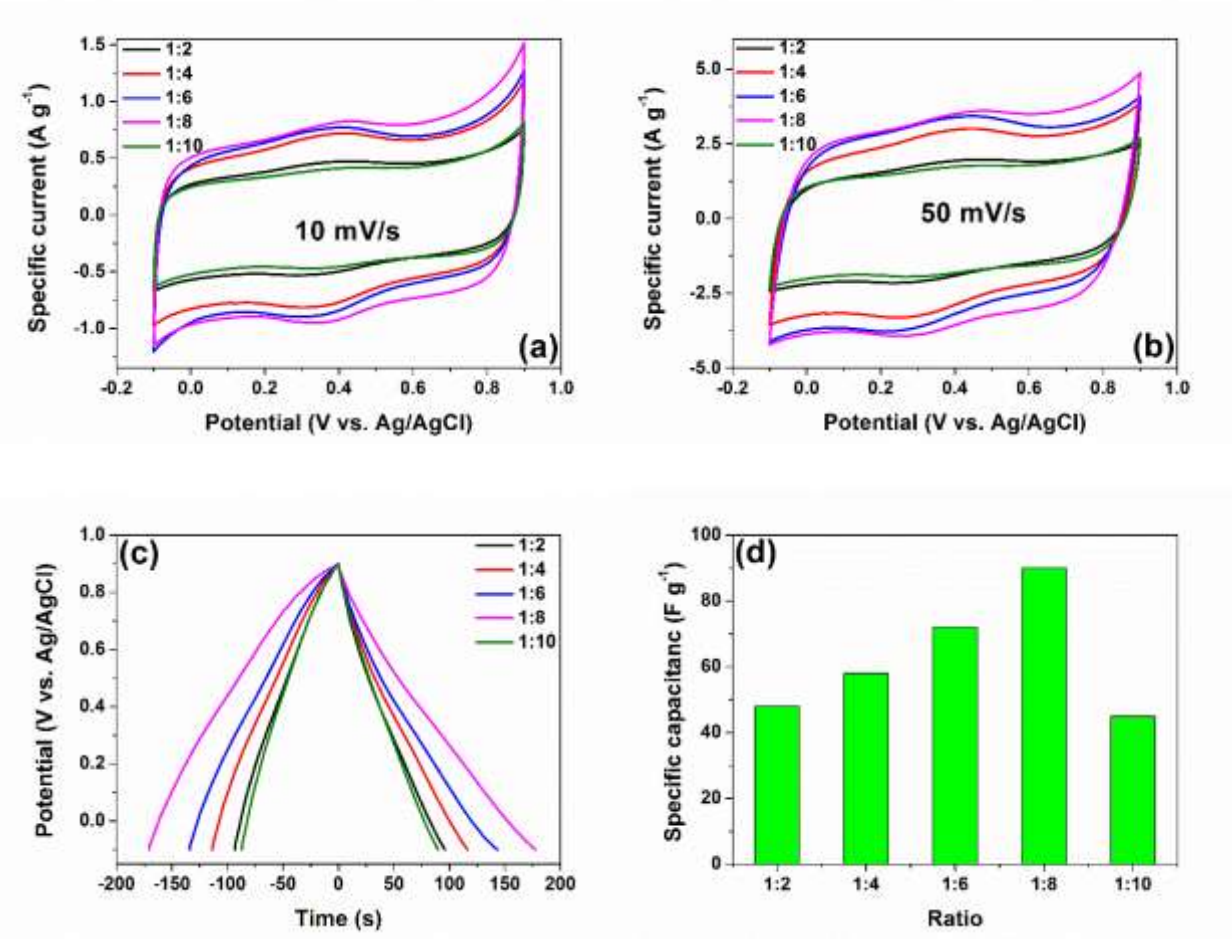

Figure 1 CV at (a) 10 mV s^{-1}, and (b) 50 mV s^{-1}, (c) GCD at 1 A g^{-1}, (d) C_{SP} as a function of the ratio of the activating agent

these groups are the origin of the observed humps due to the Faradaic characteristics. Figure 1 (c) shows the galvanostatic cycling with potential limitation (GCPL) measurement for all samples indicating ideal double-layer storage with an almost symmetric triangular galvanostatic charge-discharge (GCD) curves. The figure clearly shows that the sample 4 with a 1:8 activation ratio had the best electrochemical performance by presenting the largest charge and discharge times. This was also confirmed by the calculated C_{SP} as presented in Figure 1 d which shows the highest C_{SP} value of 90 F g^{-1} for sample 4. The order of the specific capacitance of the samples is reported as follows: sample 4 (1:8) > sample 3

(1:6) > sample 2 (1:4), sample 1 (1:2) and sample 5 (1:10). To confirm this trend, the experiment was repeated in a neutral electrolyte and the results are presented in figure S4 in the supporting information (SI). Similar results were also obtained with sample 4 clearly proving to be the best sample in 1 M KNO_3 electrolyte. However, a higher current response which is indicative of better capacitive performance was observed for samples tested in the acidic medium which led to further characterization being carried out using the acidic electrolytes.

The CV of sample 4 was performed at different sweep rate from 5–100 mV s^{-1} as shown in Figure 2 (a). The CV shapes are quasi rectangular and maintains the shapes as the scan rates increases indicating quick charge transport mechanism of the electrodes and is characteristic of highly capacitive and reversible electrochemical performance of the carbon electrodes in the acidic medium, suggesting a double layer mechanism with very small humps observed indicating partial Faradic behaviour as stated earlier. At a high scan rate of 100 mV s^{-1}, the CV curve is still partially rectangular indicative of good electrochemical performance with a good charge propagation mechanism. The GCD at different current densities also evidently confirm the double layer mechanism of the electrodes exhibiting nearly symmetric charge-discharge profiles over the potential windows as current densities increases from 0.25 to 5 A g^{-1}. The C_{SP} for the electrode was calculated from both the CV and the GCD plots according to the equations 1 and 2 with the results presented in Figure 2 (c) and 2 (d). From Figure 2 (c), a C_{SP} of 92 F g^{-1} was obtained at 5 mV s^{-1} and this remained ~66 F g^{-1} at 100 mV s^{-1} indicating rate capability retention of 72%. Similarly, a C_{SP} of 111 F g^{-1} was obtained at 0.25 A g^{-1} and 70 F g^{-1} at 5 A g^{-1} indicating a retention of 63% of its initial C_{SP} value at 5 A g^{-1}. The sample was further tested in 1 M H_2SO_4 and 1 M KNO_3 to evaluate the performance in a neutral electrolyte as shown in Figure S5 (a) and (b) with a C_{SP} of ~65 F g^{-1}

at 0.4 A g^{-1} for the 1 M KNO_3 aqueous electrolyte and figure S6 (c) and (d) with a C_{SP} of ~40 F g^{-1} at 0.25 A g^{-1} for the same sample in 1 M H_2SO_4. However, the electrochemical performance and current response were low when compared with results from 1 M HNO_3. The better performance in the 1 M HNO_3 could be due to the smaller sizes of the bare and hydrated ion sizes which are similar to the size of the pores of in the carbon material used.

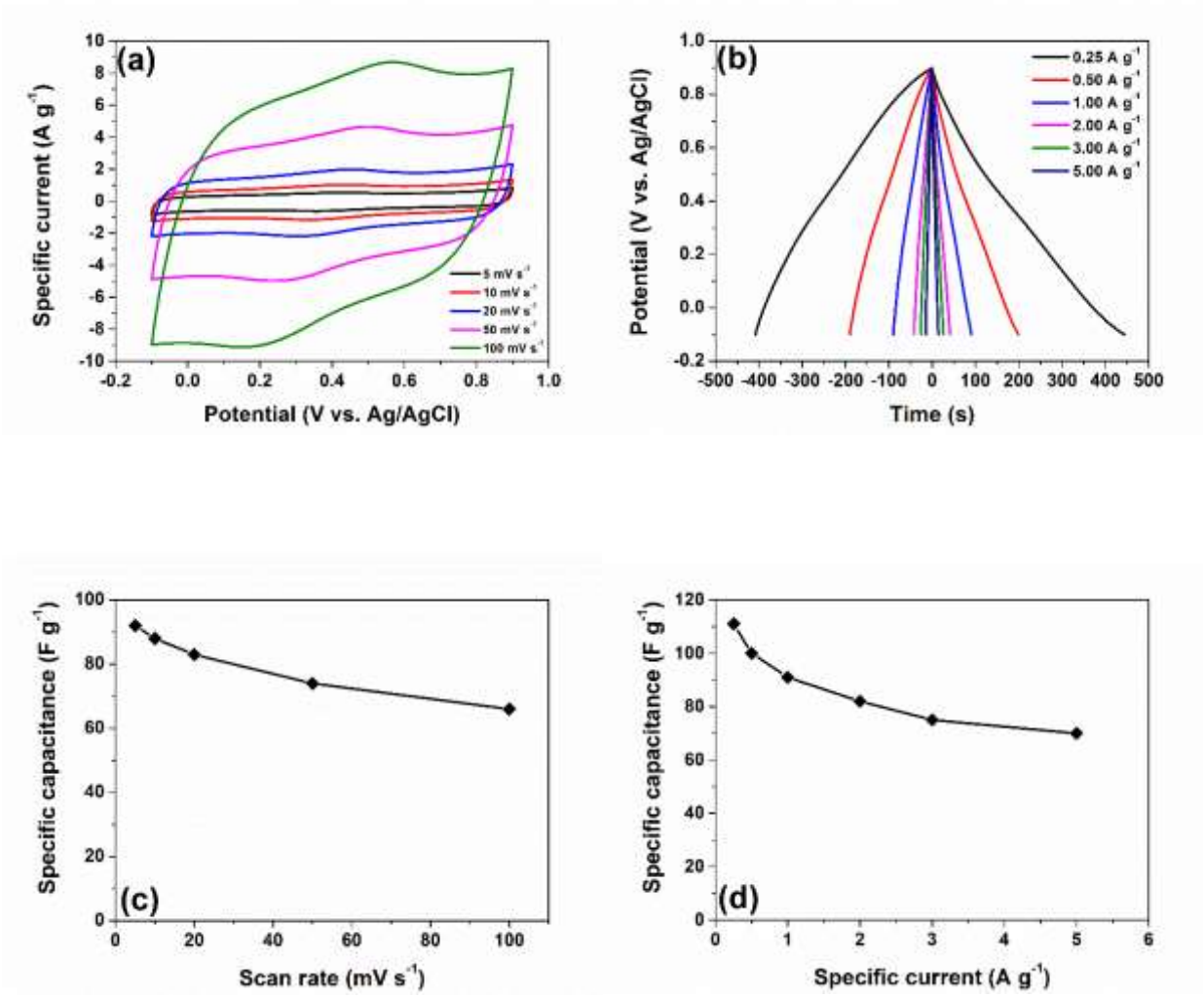

Figure 2 Electrochemistry of the optimized 1:8 AC (a) CV at different scan rate (b) the GCD at different current densities (c) C_{SP} vs. scan rate and (d) C_{SP} vs. specific current.

To further enhance the electrochemical performance of the material, redox additives were introduced into the electrolytes to enhance the charge storage capacity. Redox active

electrolytes undergo fast electron kinetics at the electrode/electrolyte interface and have been shown to be reversible within the chosen potential window and are non-toxic for industrial scale production [21]. Electrolytes which exhibit redox activity have been classified as follows; (1) redox additive–liquid electrolytes, (2) redox active liquid electrolytes and (3) redox additive–polymer gel electrolytes. Innovative research in this field explored the quinone family as additive in aqueous electrolyte [22]. Since then several redox active materials such as iodide/bromide [23,24], quinones [25,26], p-phenylamide [27,28], and transition metal ion complexes [29] have been explored to improve the electrochemical performance of supercapacitors. Thus, the addition of potassium ferricyanide ($K_3[Fe(CN)]_6$) to the aqueous electrolyte significantly improved the performance of our material due to redox reaction on the surface of the electrodes [30]. The optimization of the concentration of the additive was performed in 1 M KNO_3 and the results are presented in the SI (Figure S5 (c) and (d)). The CV curves show a pair of redox peaks which are assigned to the reversible reaction involving electron transfer according to the following equation [31]

$$[Fe(CN)_6]^{4-} \leftrightarrows [Fe(CN)_6]^{3-} + e^- \quad (7)$$

However, with increasing concentration of $K_3[Fe(CN)]_6$ in 1 M KNO_3, an increasing peak current was observed from 0.1 M to 1 M in the CV measurement and increasing discharge time as shown in Figure S4 (c) and (d) of the SI. Similarly, comparing the peak current response of the electrode in both 1 M KNO_3 and 1 M HNO_3 (Fig S5 a) and (Fig S6 a), the acid medium showed superior current behavior, hence the acid medium was used for further characterization of sample 4 with respect to the addition of redox-active additive. The redox-active additive were also tested in 1 M H_2SO_4.

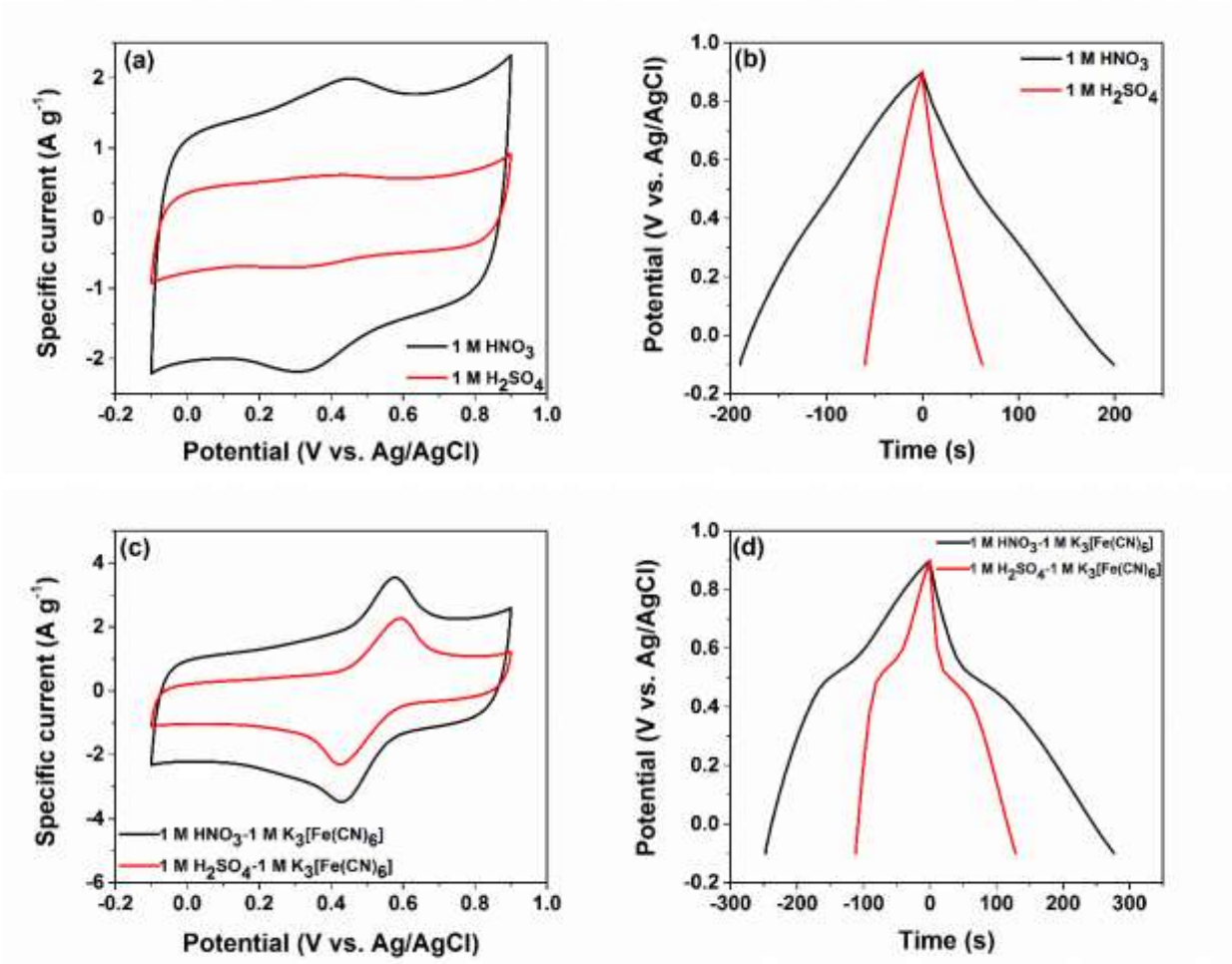

Figure 3 Figure 3 Comparison between 1 M HNO_3 and 1 M H_2SO_4, (a) CV at 20 mV s^{-1} (b) the GCD at 0.25 A g^{-1} comparison between 1 M H_2SO_4 - 1 M $K_3Fe(CN)_6$ and 1 M HNO_3 - 1 M $K_3Fe(CN)_6$ (c) CV at 20 mV s^{-1}, (d) the GCD at 0.25 A g^{-1}

Figure 3 (a) and (b) compares CV at 20 mV s^{-1} and the GCD at 0.25 A g^{-1} in 1 M HNO_3 and 1 M H_2SO_4 from -0.1 V to +0.9 V vs. Ag/AgCl evidently the nitric acid electrolyte show superior current response compared to the sulphuric acid. Similarly, figure 3 (c) and (d) shows the comparison when 1 mL of 1 M $K_3[Fe(CN)]_6$ had been added to the acidic media. Obviously, the addition clearly improve the storage capacity by combining EDL behavior with a characteristic double layer behavior with a constant capacitance, while a pair of redox peaks

is observed signifying a significant contribution to the total double layer capacitance. Most importantly the CV in the redox electrolyte mimics the shape in the acid electrolyte hinting that the additive does not increase the resistance of the electrode but increases the capacity. Figure 3 (d) also compares the GCD at a 0.25 A g^{-1} evidently the addition clearly improve the storage capacity by combining EDL behavior with a characteristic triangular shape from -0.1 V to +0.9 V vs. Ag/AgCl is related to redox reaction represented in equation 7. Hence considering the non-linearity of the GCD the performance of the electrode will be expressed in terms of capacity (mAh g^{-1}) rather than the capacitance (F g^{-1}) which will overestimate the performance [14]. Furthermore, taking into account the current response and that the nitric acid exhibited a better electrochemical performance, further electrochemical measurement will be carried out in the 1 M HNO_3 - 1 M $K_3Fe(CN)_6$.

Figure 4 (a) and (b) compares the CV and GCD plot of sample 4 in the two electrolytes at 20 mV s^{-1} and of 0.25 A g^{-1} with the acid electrolyte showing the double layer behavior with a constant capacitance, while a pair of redox peaks is observed when the additive Figure 4 (c) shows the CV at different scan rates, the peak current response increases with increasing scan rate and becomes broad at 50 and 100 mV s^{-1}. The distinct redox peak pair validates a direct electron transfer between AC electrode and redox species [30]. As the scan rate increases, the anodic peak shifts towards the positive potential while the cathodic peak shifts to the negative potential, signifying a quasi-reversible kinetics. The relationship between square root of the scan rate and peak currents is presented in Figure S7 (a), showing a linear relation with increasing scan rate indicating that the electrochemical reaction is a diffusion-controlled process. This affirms the fast kinetics of the system which is always due to the fast scan rate at which electrons diffuse at the interface of the liquid and electrode. The GCD curves at different current densities from (0.25 to 5 A g^{-1}) exhibit two

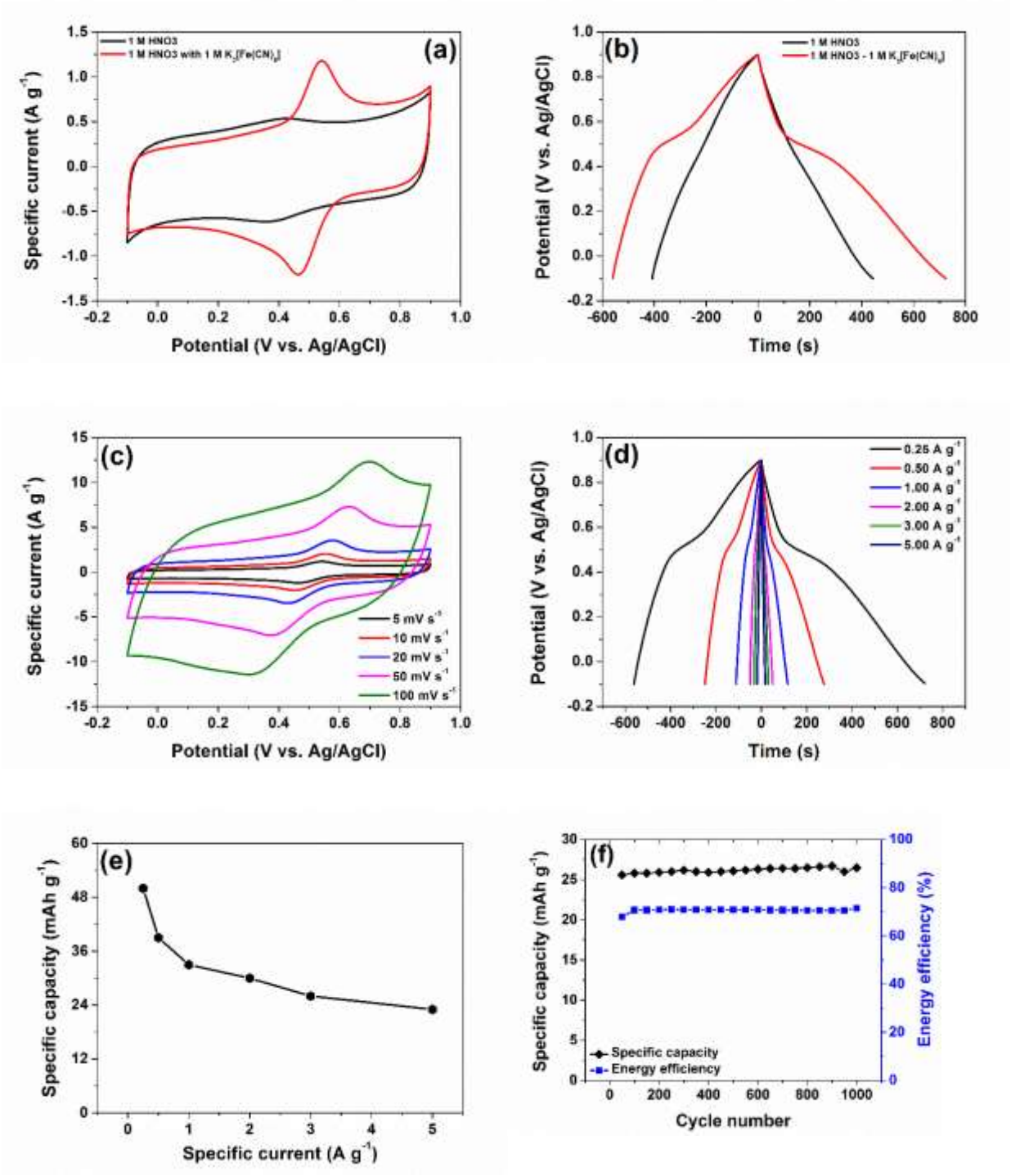

Figure 4 Comparison between 1 M HNO_3 and 1 M HNO_3 - 1 M $K_3Fe(CN)_6$ (a) CV at 20 mV s^{-1} (b) the GCD at 0.25 A g^{-1}, (c) CV at different scan rate, (d) GCD at different current densities in 1 M HNO_3-1 M $K_3Fe(CN)_6$ (e) Discharge capacity as a function of specific current and (f) Capacity retention and energy efficiency vs. cycle number.

domains: the double layer behavior after the IR drop up until 0.5 V followed by the curved region located below 0.5 V (vs. Ag/AgCl) corresponding to charge storage from the redox process as observed in Figure 4 (d). The discharge capacities (Q_D) were estimated from this curves using equation 3. The capacities values as a function of the current densities are presented in Figure 4 (e) with a maximum capacity of 50 mAh g^{-1} at 0.25 A g^{-1} and 23 mAh g^{-1} at 5 A g^{-1}. The double layer capacitance is at the higher potential while the improved performance observed is governed by the Faradaic behavior at a lower potential. In order to compare our results with other carbon materials derived from waste tyres, the C_{SP} was estimated using $C_{\mathrm{SP}} = 2E_{\mathrm{D}}/mU_{\mathrm{max}}^2$, where E_D is the discharge energy obtained by integrating the discharge curve as shown in equation 8 [14] where U_{max} is the maximum potential window.

$$E_{\mathrm{D}} = I\int_{U_{\mathrm{max}}}^{U_{\mathrm{min}}} U(t)dt \qquad 8$$

In comparison to the results obtained in the pure aqueous electrolyte, at 0.25 A g^{-1}, a specific capacity of 50 mAh g^{-1} corresponds to 140 F g^{-1} signifying an increase of ~30 F g^{-1} from the original 111 F g^{-1} obtained. The enhanced capacitive performances most likely results from the lower resistance facilitated by the rapid electron transfer in the electrode, which will be presented by the EIS analysis shortly. This value can be seen as an improvement on the specific capacitance of pure carbon materials when compared to literature. For example, a specific capacitance of 135 F g^{-1} [2] and 106 F g^{-1} [11] were recently reported for the activated carbon derived from waste tyre with KOH pellets and H_3PO_4 as an activating agents, respectively. Considering the fact the GCD is non-linear the energy efficiency, (η_E) would be more useful rather than the coulombic efficiency. The (η_E) was calculated using equation 9 [14],

$$\eta_{\mathrm{E}} = E_{\mathrm{D}}/E_{\mathrm{C}} \qquad 9$$

where $E_{\mathrm{D}}\ and\ E_{\mathrm{C}}$ are the areas under the charge and discharge curves respectively obtained using equation 8. Using this equation the energy efficiency and the corresponding specific capacity at every 50 cycles at 3 A g^{-1} was obtained. The specific capacity was maintained throughout the cycling process with a 70% energy efficiency after 1000 cycles as shown in Figure 4 (f). In order to make a direct comparison between the stability of the electrodes in 1 M HNO3 and 1 M HNO_3-$K_3Fe(CN)_6$, the capacity values obtained in the redox mediated electrolyte were converted to capacitance since the electrodes in 1 M HNO_3 exhibited pure EDLC capacitive behaviour hence better to compare them in the same unit. As shown in Figure S7 (b) both electrolytes were stable throughout the cycling with higher capacitance values obtained in the redox mediated electrolyte at the same specific current.

As much as the enhanced electrochemical performance by the addition of 1 M $K_3Fe(CN)_6$ has been noted, this should not be at the expense of the resistance of the electrodes. Thus, the enhanced and rapid electron transfer in the electrodes was investigated by EIS studies. The Nyquist plot presented in Figure 5 (a) exhibited a small arc at the high-frequency range suggesting a low charge-transfer resistance, followed by a linear line in the low-frequency range corresponding to ideal capacitive behavior resulting from the formation of EDL phenomenon, usually at this frequency, the ions can easily diffuse into the micropores of the electrodes [32]. The intercept on the *x*-axis in the high-frequency region represent the equivalent series resistance (ESR) with the value of 3.2 Ω, and 2.7 Ω in 1 M HNO_3 and 1 M HNO_3 - 1 M $K_3Fe(CN)_6$ respectively. These values are a combination of the solution resistance, the ionic resistance of the electrolyte, the intrinsic resistance of the active materials and the resistance at the interface between the active electrode material and the

current collector. The improved ESR value in the redox-based electrolyte is attributed to the fast electron kinetics and possibly increased electrolyte conductivity. The decrease in diffusion length in the impedance indicates the ease with which the ion move and penetrate into pores of the porous carbon electrodes.

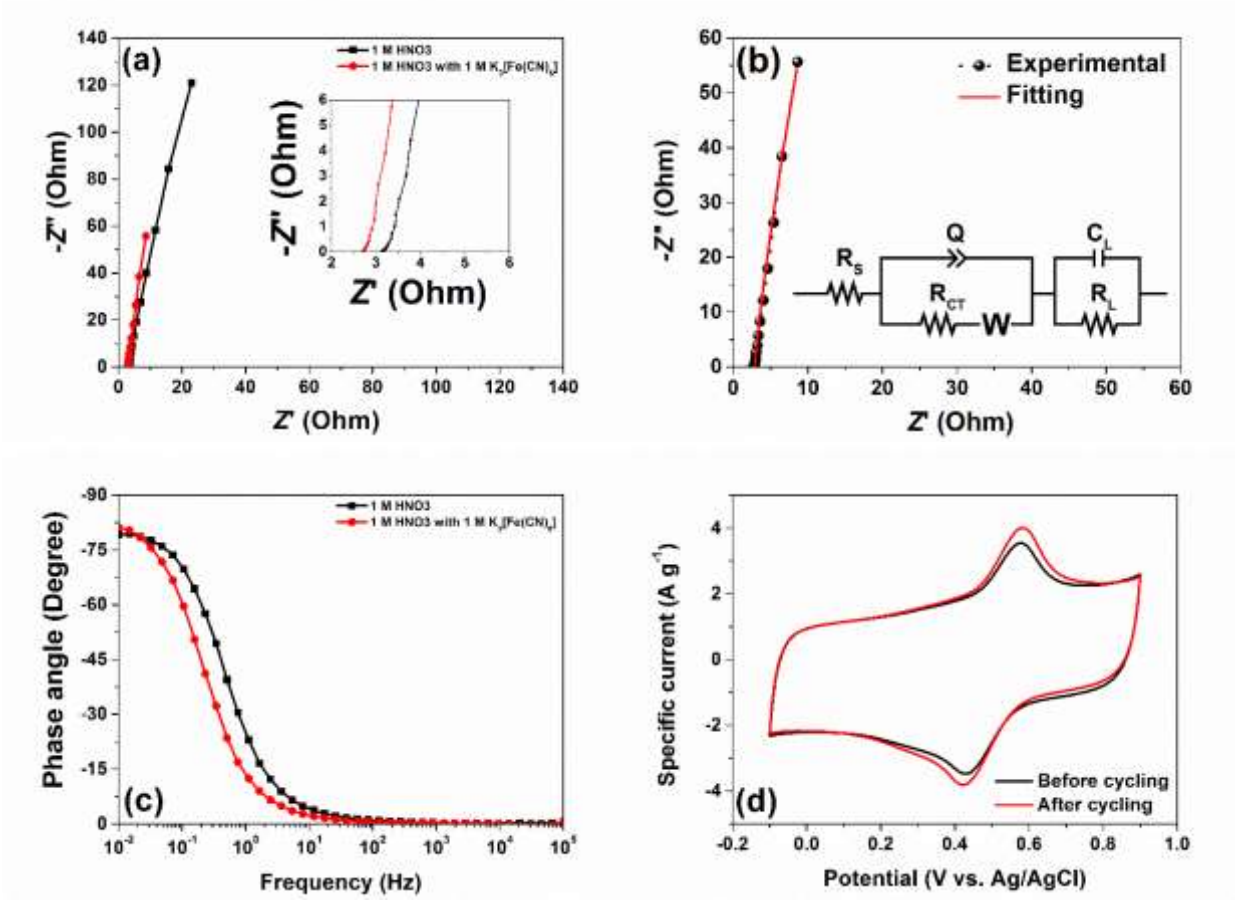

Figure 5 (a) EIS and (b) EIS fitting and equivalent circuit diagram (c) Bode phase angle in 1 M HNO_3 and 1 M HNO_3 - 1 M $K_3Fe(CN)_6$ (d) cyclic voltammetry at 20 mV s^{-1} in 1 M HNO_3 - 1 M $K_3Fe(CN)_6$ before and after cycling.

The Nyquist plot fitting and circuit shown in Figure 5 (b) consists of the ESR (R_S) which is in series with constant phase element (Q), and is placed in parallel with the Charge transfer resistance (R_{CT}) which is placed in series with the Warburg (W). The double layer capacitive element (C_L) is placed in parallel with the leakage resistance (R_L). The presence of a leakage component is tentatively ascribe

to the diffusion processes taking place at electrodes due to the presence of functional groups and oxygen at high frequency which could give rise to evolution of gases. The ESR value obtained from the fitting is 2.7 Ω which is close to the values obtained experimentally and signifies an excellent fit with the experimental data. The n-values obtained from the fitting of the Nyquist plots is 0.95 indicating a capacitive behavior. Figure S8 in the supplementary information also show the fitting and circuit diagram in the 1 M HNO_3 electrolyte alone exhibiting similar behavior to when the additive was added. This affirms a good fittings with negligible error margin. A summary of the fitting parameters from the experimental impedance spectra is presented in table S2 of the supporting information. Figure 5 (c) presents the Bode phase angles in both 1 M HNO_3 and 1 M HNO_3 – 1 M $K_3[Fe(CN)_6]$ electrolytes and correspond to ~-80° and -81°, respectively which are close to values for an ideal capacitor (~-90°). To test the stability of the electrode, CV measurement was performed after cycling and the result obtained is presented in Figure 5 (d). The CV curves at 20 mV s^{-1} before and after cycling show no significant capacitance fade rather a small improvement in current response was observed which corroborated the result obtained in Figure 4 a, indicating that the electrode is stable in the redox-mediated electrolyte.

4. Conclusion

AC were prepared from waste tyres using a mild alkaline salt potassium carbonate (K_2CO_3) as the activating agent. Electrodes fabricated exhibited a C_{SP} of 90 F g^{-1} at 0.25 A g^{-1} in a 1 M HNO_3 acidic electrolyte. The value was improved by the introduction of an additive (1 M $K_3Fe(CN)_6$) into the acid electrolyte. The redox mediated electrolyte provides rapid electrons transfer thus improving the performance to a capacity of 50 mAh g^{-1} with the energy efficiency of 70% after 1000 cycles. The results demonstrates mutual behavior between $K_3Fe(CN)_6$ and HNO_3 outperforming the result obtained in the acid medium.

Acknowledgments

This research is supported by the South African Research Chairs Initiative of the Department of Science and Technology and National Research Foundation of South Africa (Grant No. 61056). The finding and conclusion or recommendation expressed in this article is that of the author(s) and the NRF does not accept any liability in this regard. A. Bello acknowledge the National research Foundation (NRF) through the SARCHI chair in Carbon Technology and the African Centres of Excellence Program, the Pan African Materials Institute (PAMI), and the African University of Science and Technology (AUST), for their travel fellowship.

References

[1] S.L. Wong, N. Ngadi, T.A.T. Abdullah, I.M. Inuwa, Current state and future prospects of plastic waste as source of fuel: A review, Renew. Sustain. Energy Rev. 50 (2015) 1167–1180.

[2] M. Boota, M.P. Paranthaman, A.K. Naskar, Y. Li, K. Akato, Y. Gogotsi, Waste Tire Derived Carbon--Polymer Composite Paper as Pseudocapacitive Electrode with Long Cycle Life, ChemSusChem. (2015).

[3] A. Undri, S. Meini, L. Rosi, M. Frediani, P. Frediani, Microwave pyrolysis of polymeric materials: Waste tires treatment and characterization of the value-added products, J. Anal. Appl. Pyrolysis. 103 (2013) 149–158.

[4] A. Undri, B. Sacchi, E. Cantisani, N. Toccafondi, L. Rosi, M. Frediani, P. Frediani, Carbon from microwave assisted pyrolysis of waste tires, J. Anal. Appl. Pyrolysis. 104 (2013) 396–404.

[5] M. Betancur, J.D. Martínez, R. Murillo, Production of activated carbon by waste tire thermochemical degradation with CO_2, J. Hazard. Mater. 168 (2009) 882–887.

[6] A. Zabaniotou, P. Madau, P.D. Oudenne, C.G. Jung, M.-P. Delplancke, A. Fontana, Active carbon production from used tire in two-stage procedure: industrial pyrolysis and bench scale activation with H_2O–CO_2 mixture, J. Anal. Appl. Pyrolysis. 72 (2004) 289–297.

[7] A.K. Naskar, Z. Bi, Y. Li, S.K. Akato, D. Saha, M. Chi, C.A. Bridges, M.P. Paranthaman, Tailored recovery of carbons from waste tires for enhanced performance as anodes in lithium-ion batteries, RSC Adv. 4 (2014) 38213.

[8] J. Wang, S. Kaskel, KOH activation of carbon-based materials for energy storage, J. Mater. Chem. 22 (2012) 23710–23725.

[9] T. Wang, S. Tan, C. Liang, Preparation and characterization of activated carbon from wood via microwave-induced $ZnCl_2$ activation, Carbon 47 (2009) 1880–1883.

[10] Q.-S. Liu, T. Zheng, P. Wang, L. Guo, Preparation and characterization of activated carbon from bamboo by microwave-induced phosphoric acid activation, Ind. Crops Prod. 31 (2010) 233–238.

[11] M. Zhi, F. Yang, F. Meng, M. Li, A. Manivannan, N. Wu, Effects of Pore Structure on Performance of An Activated-Carbon Supercapacitor Electrode Recycled from Scrap Waste Tire, ACS Sustain. Chem. Eng. 2 (2014) 1592–1598.

[12] E. Raymundo-Pinero, P. Azais, T. Cacciaguerra, D. Cazorla-Amorós, A. Linares-Solano, F. Béguin, KOH and NaOH activation mechanisms of multiwalled carbon nanotubes with different structural organisation, Carbon 43 (2005) 786–795.

[13] W. Zhang, C. Ma, J. Fang, J. Cheng, X. Zhang, S. Dong, L. Zhang, Asymmetric electrochemical capacitors with high energy and power density based on graphene/CoAl-LDH and activated carbon electrodes, RSC Adv. 3 (2013) 2483.

[14] A. Laheäär, P. Przygocki, Q. Abbas, F. Béguin, Appropriate methods for evaluating the efficiency and capacitive behavior of different types of supercapacitors, Electrochem. Commun. 60 (2015) 21–25.

[15] Z. Ni, T. Yu, Z. Luo, Y. Wang, L. Liu, Probing charged impurities in suspended graphene using Raman spectroscopy, ACS Nano. 3 (2009) 569–574.

[16] M.J. Madito, A. Bello, J.K. Dangbegnon, C.J. Oliphant, W.A. Jordaan, T.M. Masikhwa, et al., Raman analysis of bilayer graphene film prepared on commercial Cu(0.5 at% Ni) foil, J. Raman Spectrosc. (2015).

[17] H. Demiral, I. Uzun, Preparation and characterization of activated carbons from poplar wood (Populus L.), Surf. Interface Anal. 42 (2010) 1338–1341.

[18] C.G. V Burgess, D.H. Everett, S. Nuttall, Adsorption hysteresis in porous materials, Pure Appl. Chem. 61 (1989) 1845–1852.

[19] M. Sevilla, A.B. Fuertes, A Green Approach to High-Performance Supercapacitor Electrodes: The Chemical Activation of Hydrochar with Potassium Bicarbonate, ChemSusChem. 9 (2016) 1880–1888.

[20] D. Adinata, W.M.A. Wan Daud, M.K. Aroua, Preparation and characterization of activated carbon from palm shell by chemical activation with K_2CO_3, Bioresour. Technol. 98 (2007) 145–149.

[21] S.T. Senthilkumar, R.K. Selvan, J.S. Melo, Redox additive/active electrolytes: a novel approach to enhance the performance of supercapacitors, J. Mater. Chem. A. 1 (2013) 12386.

[22] S. Roldán, C. Blanco, M. Granda, R. Menéndez, R. Santamaría, Towards a Further Generation of High-Energy Carbon-Based Capacitors by Using Redox-Active Electrolytes, Angew. Chemie Int. Ed. 50 (2011) 1699–1701.

[23] S. Yamazaki, T. Ito, M. Yamagata, M. Ishikawa, Non-aqueous electrochemical capacitor utilizing electrolytic redox reactions of bromide species in ionic liquid, Electrochim. Acta. 86 (2012) 294–297.

[24] G. Lota, K. Fic, E. Frackowiak, Alkali metal iodide/carbon interface as a source of pseudocapacitance, Electrochem. Commun. 13 (2011) 38–41.

[25] Y. Tian, R. Xue, X. Zhou, Z. Liu, L. Huang, Double layer capacitor based on active carbon and its improved capacitive properties using redox additive electrolyte of anthraquinonedisulphonate, Electrochim. Acta. 152 (2015) 135–139.

[26] S. Roldán, M. Granda, R. Menéndez, R. Santamaría, C. Blanco, Mechanisms of Energy Storage in Carbon-Based Supercapacitors Modified with a Quinoid Redox-Active Electrolyte, J. Phys. Chem. C. 115 (2011) 17606–17611.

[27] H. Yu, J. Wu, L. Fan, Y. Lin, S. Chen, Y. Chen, J. Wang, M. Huang, J. Lin, Z. Lan, others,, Application of a novel redox-active electrolyte in MnO_2-based supercapacitors, Sci. China Chem. 55 (2012) 1319–1324.

[28] Z.J. Zhang, Y.Q. Zhu, X.Y. Chen, Y. Cao, Pronounced improvement of supercapacitor capacitance by using redox active electrolyte of p-phenylenediamine, Electrochim. Acta. 176 (2015) 941–948.

[29] Q. Li, K. Li, C. Sun, Y. Li, An investigation of Cu^{2+} and Fe^{2+} ions as active materials for electrochemical redox supercapacitors, J. Electroanal. Chem. 611 (2007) 43–50.

[30] Y. Tian, M. Liu, R. Che, R. Xue, L. Huang, Cooperative redox-active additives of anthraquinone-2,7-disulphonate and $K_4Fe(CN)_6$ for enhanced performance of active carbon-based capacitors, J. Power Sources. 324 (2016) 334–341.

[31] J. Lee, S. Choudhury, D. Weingarth, D. Kim, V. Presser, High Performance Hybrid Energy Storage with Potassium Ferricyanide Redox Electrolyte, ACS Appl. Mater. Interfaces. 8 (2016) 23676–23687.

[32] Y.-R. Nian, H. Teng, Nitric acid modification of activated carbon electrodes for improvement of electrochemical capacitance, J. Electrochem. Soc. 149 (2002) A1008--A1014.